

Compound Guided Waves That Mix Characteristics of Surface-Plasmon-Polariton, Tamm, Dyakonov–Tamm, and Uller–Zenneck Waves

Francesco Chiadini,¹ Vincenzo Fiumara,² Antonio Scaglione,¹ and Akhlesh Lakhtakia³

¹Department of Industrial Engineering, University of Salerno, via Giovanni Paolo II,
132 - Fisciano (SA), 84084, Italy

²School of Engineering, University of Basilicata, Viale dell’Ateneo Lucano 10, 85100 Potenza, Italy

³Department of Engineering Science and Mechanics, Pennsylvania State University,
University Park, PA 16802–6812, USA

Abstract. Solutions of the boundary-value problem for electromagnetic waves guided by a layer of a homogeneous and isotropic (metal or dielectric) material sandwiched between a structurally chiral material (SCM) and a periodically multi-layered isotropic dielectric (PMLID) material were numerically obtained and analyzed. If the sandwiched layer is sufficiently thick, the two bimaterial interfaces decouple from each other, and each interface may guide one or more electromagnetic surface waves (ESWs) by itself. Depending on the constitution of the two materials that partner to form an interface, the ESWs can be classified as surface-plasmon-polariton (SPP) waves, Tamm waves, Dyakonov–Tamm waves, or Uller–Zenneck waves. When the sandwiched layer is sufficiently thin, the ESWs for single bimaterial interfaces coalesce to form compound guided waves (CGWs). The phase speeds, propagation distances, and spatial profiles of the electromagnetic fields of CGWs are different from those of the ESWs. The energy of a CGW is distributed in both the SCM and the PMLID material, if the sandwiched layer is sufficiently thin. Some CGWs require the sandwiched layer to have a minimum thickness. Indeed, the coupling between the two faces of the sandwiched layer is affected by the ratio of the thickness of the sandwiched layer to the skin depth in that material and the rates at which the fields of the ESWs guided individually by the two interfaces decay away from their respective guiding interfaces.

1 Introduction

Several different kinds of electromagnetic surface waves (ESWs) exist. Perhaps the first ever analytical treatment was of an ESW guided by the planar interface of air and seawater, published in his doctoral dissertation by Uller in 1903 [1]. As Wait [2] recounted in a review of ground-wave propagation, that was also the time when Tesla [3] conjectured that radio waves are guided by the air/earth interface, a proposition analyzed by Zenneck [4] in 1907 and by Sommerfeld [5, 6, 7] in several papers thereafter. The ESWs bound to the planar interface of two homogeneous dielectric materials of which one is dissipative are called Zenneck waves, but should be more properly called Uller–Zenneck waves [8].

ESWs called surface-plasmon-polariton (SPP) waves are guided by the planar interface of two isotropic and homogeneous materials, one of which has a relative permittivity with negative real part (usually, a metal) and the other whose relative permittivity has positive real part (usually, a dielectric material). SPP waves became a topic of research after the energy losses of electrons impinging on a metal film were explained in 1957 in terms of electronic-plasma oscillations occurring at the film’s surfaces [9]. But SPP waves cannot be excited by shining light directly at either a dielectric film lying atop a metal film or a metal film lying atop a dielectric film. The reflectance of a parallel-polarized plane wave from a thin aluminum film deposited on the hypotenuse of a right-angled glass prism was shown in 1959 to exhibit a sharp dip as the angle of incidence exceeded the critical angle for a planar glass/air interface [10]. The reflectance dip was related to the excitation of an SPP wave in 1968 [11, 12], and an explosive expansion of research on applications of SPP waves started thereafter [13, 14, 15]. The excitation of a multiplicity of SPP waves at a specific frequency is possible if the dielectric partnering material is periodically non-homogeneous (on the order of

wavelength) in the direction normal to the interface [16, 17]. In this case, even though all SPP waves are excited at the same frequency, they can differ for polarization state, phase speed, attenuation rate, and field profile; furthermore, the dielectric partnering material can even be anisotropic [18, 16].

Most SPP waves do not propagate long distances along the interface plane, because metals are dissipative. If both partnering materials are weakly dissipative dielectric materials, the propagation distance would be enhanced. Indeed, the Tamm wave was predicted in 1977 to be guided by the interface of two isotropic dielectric materials, at least one of which was periodically non-homogeneous in the direction perpendicular to the interface [19]. The experimental observation of Tamm waves followed in 1978 [20], and their application to optical sensing has been subsequently demonstrated [21, 22].

A few years later, Marchevskii *et al.* [23] and Dyakonov [24] predicted an ESW guided by the interface of two homogeneous dielectric materials, at least one of which is anisotropic. Experimental verification came only in 2009, when Takayama *et al.* were able to excite a Dyakonov wave guided by the interface of a liquid and a biaxial dielectric crystal [25]. But the Dyakonov wave propagates in very narrow ranges of directions ($\lesssim 1$ deg out of a maximum of 360 deg) in the interface plane [26], and is difficult to detect. The insertion of a 10–20-nm thick dielectric sheet between an anisotropic and an isotropic material can enhance the range of directions of propagation [27].

In 2007 Lakhtakia and Polo [28] proposed an ESW that is guided by the interface of two dielectric materials, one of which is isotropic and homogeneous, and the other is both anisotropic and periodically non-homogeneous in the direction perpendicular to the interface plane. Combining the attributes of both Tamm and Dyakonov waves, this surface wave was named a Dyakonov–Tamm wave. The angular sectors permitting the propagation of Dyakonov–Tamm waves are so large as to often cover the entire 360 deg available [16]. Dyakonov–Tamm waves are also expected to be useful for optical sensing [29].

Two SPP waves can be *compounded* when a metal layer of thickness L is sandwiched between two half spaces filled with isotropic, homogeneous dielectric materials [30, 31, 32]. But L must not be significantly larger than the skin depth δ in the metal, or the coupling between the two dielectric/metal interfaces vanishes and each of the two interfaces by itself guides an SPP wave that will not coalesce with the other SPP wave. The compound guided wave (CGW) can propagate over longer distances than an SPP wave guided by a single metal/dielectric interface. Recently, we examined the CGWs guided by a thin metal layer sandwiched between a homogeneous isotropic dielectric (HID) material and either a periodically multi-layered isotropic dielectric (PMLID) material [33] or a structurally chiral material (SCM) [34], all dielectric non-metallic materials being assumed to have negligible dissipation. We found that a multiplicity of CGWs with plasmonic and polaritonic constituents can propagate bound to both metal/dielectric interfaces with energy distributed in both the dielectric materials if the metal layer is sufficiently thin. Long-range CGWs are also guided by a thin metal layer inserted in a periodically non-homogeneous anisotropic material such that the direction of non-homogeneity is the same as the thickness direction of the metal film [35] with non-homogeneity on the wavelength scale; furthermore, CGWs resembling Dyakonov–Tamm waves in their characteristics are guided, if the sandwiched metal is replaced by an isotropic dielectric material [36]. Finally, CGWs that fuse together the characteristics of SPP waves and Dyakonov waves have been theoretically shown to excited via a uniaxial dielectric layer inserted between a HID material and a metal [37]. Thus, planar multi-interface structures offer the possibility of CGWs that mix the characteristics of two (or more) ESWs.

With our interest lying in the compounding of ESWs that require at least one of the partnering materials to be periodically non-homogeneous normal to the direction of propagation, in the present paper, we address and solve the boundary-value problem of the propagation of a CGW guided by a layer of a homogeneous and isotropic (metal or dielectric) material sandwiched between an SCM and a PMLID material. Thereby, compounding of the characteristics of SPP waves, Tamm waves, Dyakonov–Tamm waves, and Uller–Zenneck waves is investigated. Let us note that the analyzed structures can be manufactured using techniques routinely used to fabricate optical thin films, especially multilayer thin films [38, 39] and sculptured thin films [40], and liquid crystals [41].

The plan of this paper is as follows: Sec. 2 provides in brief the boundary-value problem for CGWs guided by a planar A/B/C structure and introduces the materials chosen as A, B, and C for the numerical results presented in Secs. 3 and 4. Section 3 provides some results for ESWs guided by the A/B, B/C, and

A/C bimaterial interfaces individually. Section 4 is devoted to numerical results for CGWs guided by the A/B/C structure and comparison with the results presented in Sec. 3. Concluding remarks follow in Sec. 5.

An $\exp(-i\omega t)$ dependence on time t is implicit, with ω denoting the angular frequency and $i = \sqrt{-1}$. The free-space wavenumber, the free-space wavelength, and the intrinsic impedance of free space are denoted by $k_0 = \sqrt{\varepsilon_0\mu_0}$, $\lambda_0 = 2\pi/k_0$, and $\eta_0 = \sqrt{\mu_0/\varepsilon_0}$, respectively, with ε_0 and μ_0 being the permeability and permittivity of free space. The speed of light in vacuum is denoted by $c_0 = \sqrt{\varepsilon_0\mu_0}$. Vectors are in boldface; dyadics are underlined twice; and Cartesian unit vectors are identified as \mathbf{u}_x , \mathbf{u}_y , and \mathbf{u}_z .

2 Theoretical Preliminaries and Materials

A schematic of the boundary-value problem for the propagation of a CGW is provided in Figure 1. A slab of material B is interposed between the half space $z < 0$ occupied by material A and the half space $z > L$ occupied by a material C. Given the wide variety of compound CGWs possible, we chose A to be a PMLID material, B to be a homogeneous and isotropic material, and C to be an SCM.

The PMLID material A has a period $\Lambda = 675$ nm with a unit cell consisting of $N = 9$ equal-thickness nondissipative dielectric layers of different silicon oxynitrides, each fabricated by plasma-enhanced chemical vapor deposition of a specific composition of silane, ammonia, and nitrous oxide [42]. The layers contain SiO_2 and SiN_x in the ratios shown in Table 1. The layer labeled $j = 1$ in the first unit cell of the PMLID material is the one closest to material B.

Table 1: **Composition and relative permittivity ε_j at $\lambda_0 = 633$ nm of the j^{th} layer in the unit cell of the chosen PMLID material [42].**

j	$\text{SiO}_2\%$	$\text{SiN}_x\%$	ε_j
1	0	100	3.9357
2	32	68	3.3033
3	40	60	3.1515
4	49	51	3.0056
5	62	38	2.7526
6	72	28	2.6143
7	82	18	2.4475
8	90	10	2.3161
9	100	0	2.1837

For all calculations reported here, material B can be either (i) a metal, specifically silver with relative permittivity $\varepsilon_{Ag} = -14.461 + i1.1936$; or (ii) a dissipative HID with $\varepsilon_{dHID} = 14.461 + i1.1936$ which was used as a nonplasmonic analog of silver; or (iii) a practically nondissipative HID, specifically a glass with relative permittivity $\varepsilon_{glass} = 2.56$.

Material C was chosen to be an SCM—specifically, a structurally right-handed chiral sculptured thin film of patinal titanium oxide with permittivity dyadic given at $\lambda_0 = 633$ nm by [34, 43]

$$\begin{aligned}
\underline{\underline{\varepsilon}}_{SCM}(z) &= \varepsilon_0 \underline{\underline{S}}_z \left(\frac{2\pi z}{P} \right) \cdot \underline{\underline{S}}_y(37.6745^\circ) \\
&\cdot (2.13952 \mathbf{u}_z \mathbf{u}_z + 3.66907 \mathbf{u}_x \mathbf{u}_x + 2.82571 \mathbf{u}_y \mathbf{u}_y) \\
&\cdot \underline{\underline{S}}_y^{-1}(37.6745^\circ) \cdot \underline{\underline{S}}_z^{-1} \left(\frac{2\pi z}{P} \right),
\end{aligned} \tag{1}$$

with

$$\begin{aligned} \underline{\underline{S}}_z(\zeta) &= \mathbf{u}_z \mathbf{u}_z + (\mathbf{u}_x \mathbf{u}_x + \mathbf{u}_y \mathbf{u}_y) \cos \zeta \\ &\quad + (\mathbf{u}_y \mathbf{u}_x - \mathbf{u}_x \mathbf{u}_y) \sin \zeta, \end{aligned} \quad (2)$$

$$\begin{aligned} \underline{\underline{S}}_y(\chi) &= \mathbf{u}_y \mathbf{u}_y + (\mathbf{u}_x \mathbf{u}_x + \mathbf{u}_z \mathbf{u}_z) \cos \chi \\ &\quad + (\mathbf{u}_z \mathbf{u}_x - \mathbf{u}_x \mathbf{u}_z) \sin \chi, \end{aligned} \quad (3)$$

and $P = 270$ nm as the period along the z axis.

We consider the CGW to be propagating parallel to the unit vector $\mathbf{u}_{prop} = \mathbf{u}_x \cos \psi + \mathbf{u}_y \sin \psi$, $\psi \in [0^\circ, 360^\circ)$, in the xy plane and decaying far away from the layer of material B. With q as the complex-valued wavenumber of the CGW, the electric and magnetic field phasors can be represented everywhere by

$$\left. \begin{aligned} \mathbf{E}(\mathbf{r}) &= \mathbf{e}(z) \exp(iq\mathbf{u}_{prop} \cdot \mathbf{r}) \\ \mathbf{H}(\mathbf{r}) &= \mathbf{h}(z) \exp(iq\mathbf{u}_{prop} \cdot \mathbf{r}) \end{aligned} \right\}. \quad (4)$$

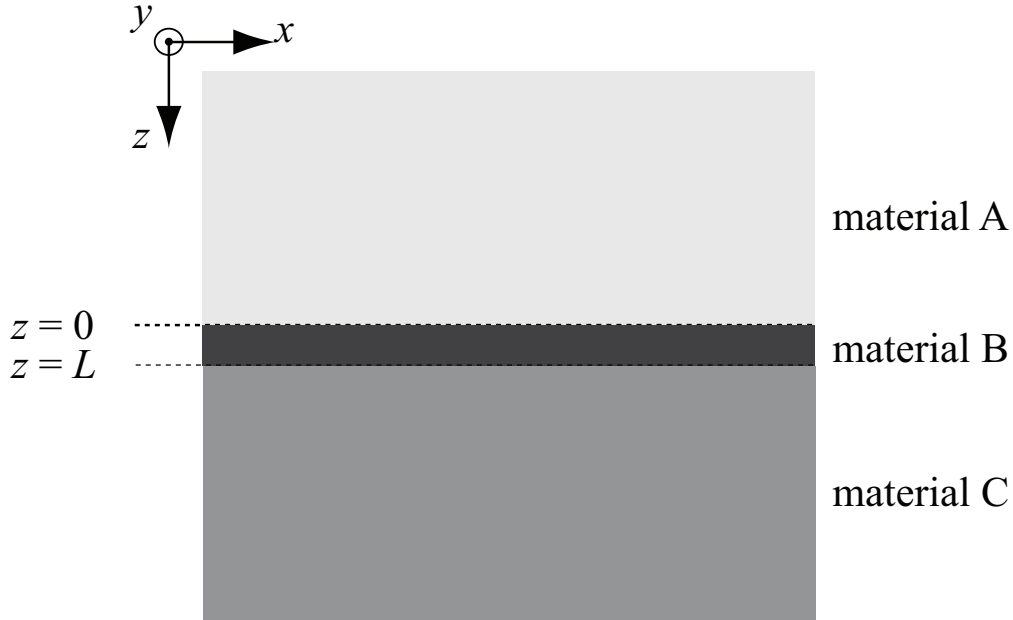


Figure 1: Schematic of the boundary-value problem to examine the propagation of CGWs.

The axial field components $e_z(z)$ and $h_z(z)$ of $\mathbf{e}(z)$ and $\mathbf{h}(z)$, respectively, can be expressed in terms of the column 4-vector [16]

$$[\mathbf{f}(z)] = [e_x(z) \quad e_y(z) \quad h_x(z) \quad h_y(z)]^T \quad (5)$$

that satisfies the matrix differential equations

$$\frac{d}{dz} [\mathbf{f}(z)] = i \left[\underline{\underline{P}}^{(\sigma)}(z) \right] \cdot [\mathbf{f}(z)], \quad \sigma = \begin{cases} \text{A}, & z < 0 \\ \text{B}, & 0 < z < L \\ \text{C}, & z > L \end{cases} \quad (6)$$

where the 4×4 matrixes $\left[\underline{\underline{P}}^{(\sigma)}(z) \right]$ can be written for materials A, B, and C. Since material B is homogeneous, the matrix $\left[\underline{\underline{P}}^{(\text{B})} \right]$ is independent of z , and we obtain

$$[\mathbf{f}(L)] = \exp \left\{ i \left[\underline{\underline{P}}^{(\text{B})} \right] L \right\} \cdot [\mathbf{f}(0)] \quad (7)$$

after solving (6) [16]. By virtue of the periodicity of both materials A, and C along the z axis, we have

$$[\mathbf{f}(0)] = \left[\underline{\underline{Q}}^{(A)} \right] \cdot [\mathbf{f}(-\Lambda)] \quad (8)$$

$$[\mathbf{f}(L+P)] = \left[\underline{\underline{Q}}^{(C)} \right] \cdot [\mathbf{f}(L)] \quad (9)$$

where each of the 4×4 matrixes $\left[\underline{\underline{Q}}^{(A)} \right]$ and $\left[\underline{\underline{Q}}^{(C)} \right]$ characterizes the optical response of one period. Whereas $\left[\underline{\underline{Q}}^{(A)} \right]$ can be calculated as the cascade of the transfer matrixes of the layers constituting one period of the PMLID material, $\left[\underline{\underline{Q}}^{(C)} \right]$ can be obtained by a piecewise uniform approximation subdividing one period of the SCM in thin slices, parallel to the plane $z = 0$, with equal thickness and spatially uniform dielectric properties [16, 40].

After the imposition of the standard boundary conditions across the interfaces $z = 0$ and $z = L$, Eqs. (7)–(9) lead to the matrix equation

$$\left[\underline{\underline{M}}(q) \right] \cdot [\mathbf{S}] = 0. \quad (10)$$

The matrix $\left[\underline{\underline{M}}(q) \right]$ is synthesized from the $\left[\underline{\underline{Q}}^{(B)} \right]$ as well as from the eigenvectors of $\left[\underline{\underline{Q}}^{(A)} \right]$ and $\left[\underline{\underline{Q}}^{(C)} \right]$, as shown in detail elsewhere [16, Sec. 3.6]. The column 4-vector $[\mathbf{S}]$ contains 4 unknown coefficients.

Equation (10) has a nontrivial solution only when the matrix $\left[\underline{\underline{M}}(q) \right]$ is singular. Therefore the dispersion equation $\det \left[\underline{\underline{M}}(q) \right] = 0$ has to be solved for q .

We numerically solved the dispersion equation to obtain the normalized wavenumbers $\tilde{q} = q/k_0$ of the CGWs. Knowing q , we can calculate the phase speed $v_{ph} = c_0/\text{Re}(\tilde{q})$ and the propagation distance $\Delta_{prop} = 1/\text{Im}(q)$ of the CGW in the direction parallel to \mathbf{u}_{prop} , where Δ_{prop} is the distance along the direction of propagation at which the wave amplitude reduces by a factor of $\exp(-1) = 0.367$ and the power density reduces by $\exp(-2) = 0.135$. The main characteristics of the CGW can be illustrated by the spatial distribution of the time-averaged Poynting vector

$$\mathbf{P}(\mathbf{r}) = \frac{1}{2} \text{Re} [\mathbf{e}(z) \times \mathbf{h}^*(z)] \exp[-2\text{Im}(q)\mathbf{u}_{prop} \cdot \mathbf{r}], \quad (11)$$

where the asterisk denotes the complex conjugate. If both materials A and C are isotropic, the CGW is either p or s polarized, and q as well as Δ_{prop} are independent of ψ (i.e., the direction of propagation in the xy plane). But, if at least one of those two materials is an SCM, then no polarization state can be assigned to the CGW [16].

We focused on CGWs that fuse together at least two ESWs of the following kinds: SPP waves, Tamm waves, Dyakonov–Tamm waves, and Uller–Zenneck waves. In order to present representative numerical results, we fixed $\lambda_0 = 633$ nm and $\psi = 30$ deg, the dependence on ψ of these CGWs being quite weak for the chosen SCM. All calculations were restricted to $0 < \text{Re}(\tilde{q}) \leq 3$ to avoid computational instabilities that emerged for $\text{Re}(\tilde{q}) > 3$.

3 ESWs guided by an A/B, B/C, or A/C bimaterial interface

In order to appreciate the characteristics of CGWs guided by two parallel bimaterial interfaces (as in Fig. 1), it is best to briefly present results for simple ESWs guided by a single bimaterial interface. Table 2 summarizes the type of ESWs guided by the planar interface of two different partnering materials: A/B, B/C, or A/C. Their relevant characteristics and the differences between ESWs of different types are discussed in the following subsections.

3.1 Planar SCM/metal interface

Two SPP-wave modes can be guided by the interface of the chosen SCM and metal, when $\psi = 30$ deg. According to Table 3, one of these two modes will propagate five times farther than the other mode, with the former possessing a higher phase speed than the latter.

Table 2: **Types of ESWs and their characteristics for the choice of partnering materials A and B.**

ESW Type	Partnering materials		Data	Number of modes	Characteristics
	A	B			
SPP	SCM	Metal	Table 3	2	No polarization state can be assigned
	PMLID material	Metal	Table 5	7	4 p - and 3 s -polarized, 2 high-phase speed
Uller-Zenneck	SCM	Dissipative HID	Table 4	2	No polarization state can be assigned
	PMLID material	Dissipative HID	Table 6	6	3 p - and 3 s -polarized, 2 high-phase speed
Tamm	SCM	nondissipative HID	–	0	–
	PMLID material	nondissipative HID	Table 7	2	1 p - and 1 s -polarized
Dyakonov-Tamm	SCM	PMLID material	–	1	No polarization state can be assigned

Table 3: \tilde{q} , v_{ph} , and Δ_{prop} for SPP waves guided by the SCM/metal interface alone for $\psi = 30$ deg.

Solution	$\text{Re}(\tilde{q})$	$\text{Im}(\tilde{q})$	v_{ph}/c_0	Δ_{prop} (μm)
1	1.18553	3.48×10^{-3}	0.84350	28.95
2	1.85217	1.77×10^{-2}	0.53991	5.69

3.2 Planar SCM/dissipative-HID interface

The planar interface of the chosen SCM and the nonplasmonic but dissipative analog of silver (with $\varepsilon_{dHID} = -\varepsilon_{Ag}^*$) by itself was found to guide two different Uller-Zenneck waves (also classifiable as Dyakonov-Tamm waves [28]) when $\psi = 30$ deg; see Table 4 for relevant data.

The substantial difference between the SPP waves in Sec. 3.1 and the Uller-Zenneck waves in this section is in the much shorter propagation distances of the latter than of the former. This difference must be due to the considerably smaller skin depth of silver ($\delta = 26.5$ nm) than of its nonplasmonic but dissipative analog ($\delta = 642$ nm). Another difference between the SPP and Uller-Zenneck waves is that, whereas the higher- v_{ph} SPP wave has the longer propagation distance, the higher- v_{ph} Uller-Zenneck wave has the shorter propagation distance.

Table 4: \tilde{q} , v_{ph} , and Δ_{prop} for Uller-Zenneck (or Dyakonov-Tamm) waves guided by the SCM/dissipative-HID interface alone for $\psi = 30$ deg.

Solution	$\text{Re}(\tilde{q})$	$\text{Im}(\tilde{q})$	v_{ph}/c_0	Δ_{prop} (μm)
1	1.06817	5.90×10^{-2}	0.93618	1.71
2	1.52148	5.58×10^{-2}	0.65725	1.81

3.3 Planar SCM/nondissipative-HID interface

The planar interface of the chosen SCM and glass by itself was not found to guide any ESW. This is not surprising because the range of the refractive index of the lossless HID material for the existence of a Dyakonov-Tamm wave is generally very small [28], and we conclude that the chosen refractive index ($= 1.6$) of glass must lie outside that range.

3.4 Planar PMLID/metal interface

The planar interface of the chosen PMLID material and silver by itself was found to guide four p - and three s -polarized SPP waves, with no dependence on ψ . These solutions are labeled as $p_{1,2,3,4}$ and $s_{1,2,3}$ in Table 5.

An increase in the number of SPP waves when the SCM is replaced by a PMLID material has been noticed earlier [44, 45]. A high-phase-speed solution ($\text{Re}\{\tilde{q}\} < 1$) [45] exists for each polarization state.

Table 5: \tilde{q} , v_{ph} , and Δ_{prop} for p - and s -polarized SPP waves guided by the PMLID/metal interface alone. Solutions with $v_{ph} > c_0$ are highlighted in bold font.

Solution	$\text{Re}(\tilde{q})$	$\text{Im}(\tilde{q})$	v_{ph}/c_0	Δ_{prop} (μm)
p₁	0.93964	5.21×10^{-4}	1.06424	193.37
p_2	1.36469	1.56×10^{-4}	0.73277	645.80
p_3	1.59093	1.49×10^{-3}	0.62856	67.61
p_4	2.27526	3.81×10^{-2}	0.43951	2.64
s₁	0.95783	1.26×10^{-3}	1.04403	79.96
s_2	1.40658	8.45×10^{-4}	0.71094	119.22
s_3	1.66592	7.57×10^{-4}	0.60027	133.08

3.5 Planar PMLID/dissipative-HID interface

The planar interface of the chosen PMLID material and the nonplasmonic but dissipative HID material by itself was found to guide two different Uller–Zenneck waves (also classifiable as Tamm waves [28]) independently of ψ ; see Table 6 for relevant data. The substantial difference between the SPP waves in Table 5 and the Uller–Zenneck waves in Table 6 is in the generally much shorter propagation distances of the latter than of the former. Again, this difference must be ascribed to the considerably smaller skin depth of silver ($\delta = 26.5$ nm) than of its nonplasmonic but dissipative analog ($\delta = 642$ nm).

Table 6: \tilde{q} , v_{ph} , and Δ_{prop} for p - and s -polarized Uller–Zenneck (or Tamm) waves guided by the PMLID/dissipative-HID interface alone. Solutions with $v_{ph} > c_0$ are highlighted in bold font.

Solution	$\text{Re}(\tilde{q})$	$\text{Im}(\tilde{q})$	v_{ph}/c_0	Δ_{prop} (μm)
p₁	0.92055	3.96×10^{-2}	1.08631	2.54
p_2	1.52861	5.52×10^{-2}	0.65419	1.83
p_3	1.71776	1.46×10^{-1}	0.58215	0.69
s₁	0.91802	6.05×10^{-2}	1.08930	1.67
s_2	1.38091	3.14×10^{-2}	0.72416	3.21
s_3	1.64373	2.68×10^{-2}	0.60837	3.76

3.6 Planar PMLID/nondissipative-HID interface

The planar interface of the chosen PMLID material and glass by itself was found to guide one p - and one s -polarized Tamm waves, without any dependence on ψ ; see Table 7 for data. Both partnering materials being nondissipative, the wavenumbers are purely real, which means that both Tamm waves can be expected to propagate for very long distances by experimentalists.

3.7 Planar SCM/PMLID interface

Only one ESW was found to be guided by the SCM/PMLID interface when $\psi = 30$ deg. Classified as a Dyakonov–Tamm wave, its normalized wavenumber $\tilde{q} = 1.77612$ and its phase speed $v_{ph} = 0.56302c_0$. Spatial variations of the Cartesian components of its time-averaged Poynting vector $\mathbf{P}(0, 0, z)$ are presented in Figure 2.

Table 7: \tilde{q} and v_{ph} for p - and s -polarized Tamm waves guided by the PMLID/glass interface alone.

Solution	\tilde{q}	v_{ph}/c_0
p_1	1.72282	0.58044
s_1	1.74660	0.57254

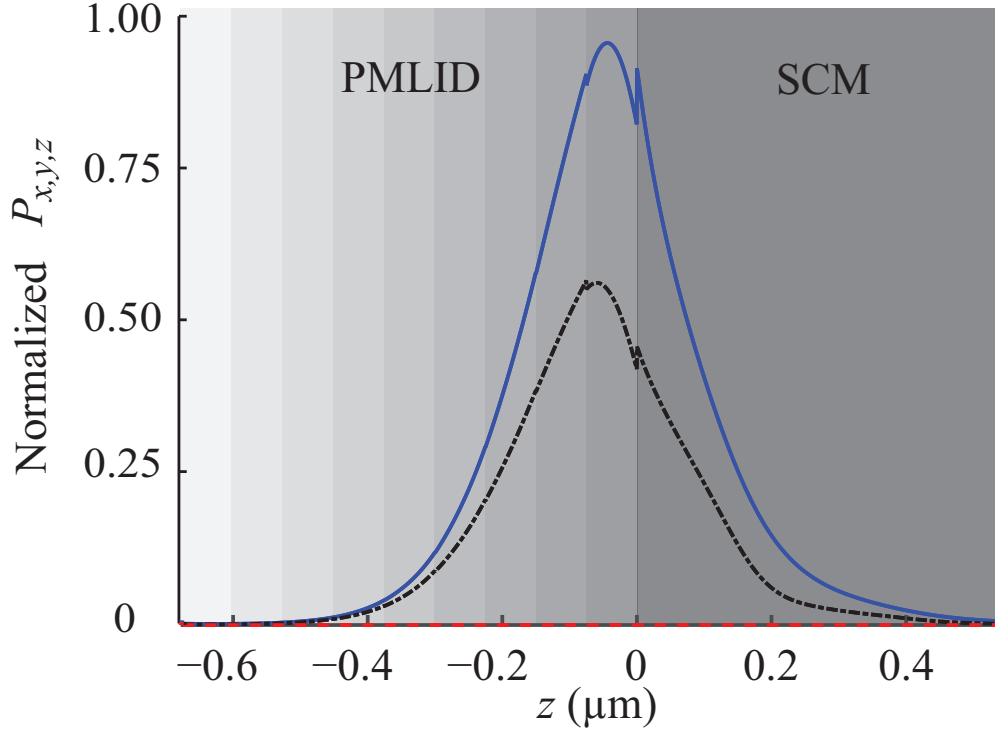


Figure 2: Spatial variations of $P_x(0,0,z)$ (blue solid lines), $P_y(0,0,z)$ (black dashed-dotted lines) and $P_z(0,0,z)$ (red dashed lines) with respect to z of the Dyakonov–Tamm wave guided by the planar SCM/PMLID interface when $\psi = 30^\circ$.

4 CGWs guided by A/B/C structure

Now let us turn to the problem schematically illustrated in Figure 1, with materials A and C being the chosen PMLID material and SCM, respectively, while material B is isotropic and homogeneous. The thickness L of the sandwiched layer was varied from $L_{min} = 0$ to $L_{max} = 120$ nm. With some degree of approximation, this problem can be practically implemented with the A/B/C structure of sufficiently large thickness and finite width interposed between two waveguide sections.

4.1 Planar PMLID/metal/SCM structure

Let us begin by choosing material B to be silver (i.e., $\epsilon_B = \epsilon_{Ag}$). Since materials A and C are dielectric, the CGWs guided by this structure must be classified as compounded from SPP waves for $L > 0$. However, this compounding is more complicated than in two predecessor papers wherein either A [34] or C [33] was isotropic and homogeneous. The number of CGWs and their wavenumbers depend on ψ due to the anisotropy of the SCM. Except in special cases, no polarization state can be assigned to any of the CGWs.

Depending on the value of $L \in (0, 120]$ nm, as many as nine different CGWs can be guided by the structure. Figures 3 and 4, respectively, show $\text{Re}(\tilde{q})$ and Δ_{prop} as functions of L , the wavenumbers q being organized into nine different branches. Solutions on branches numbered 1 and 2 in the figures have phase speeds exceeding c_0 , whereas the other seven branches have solutions with phase speeds below c_0 .

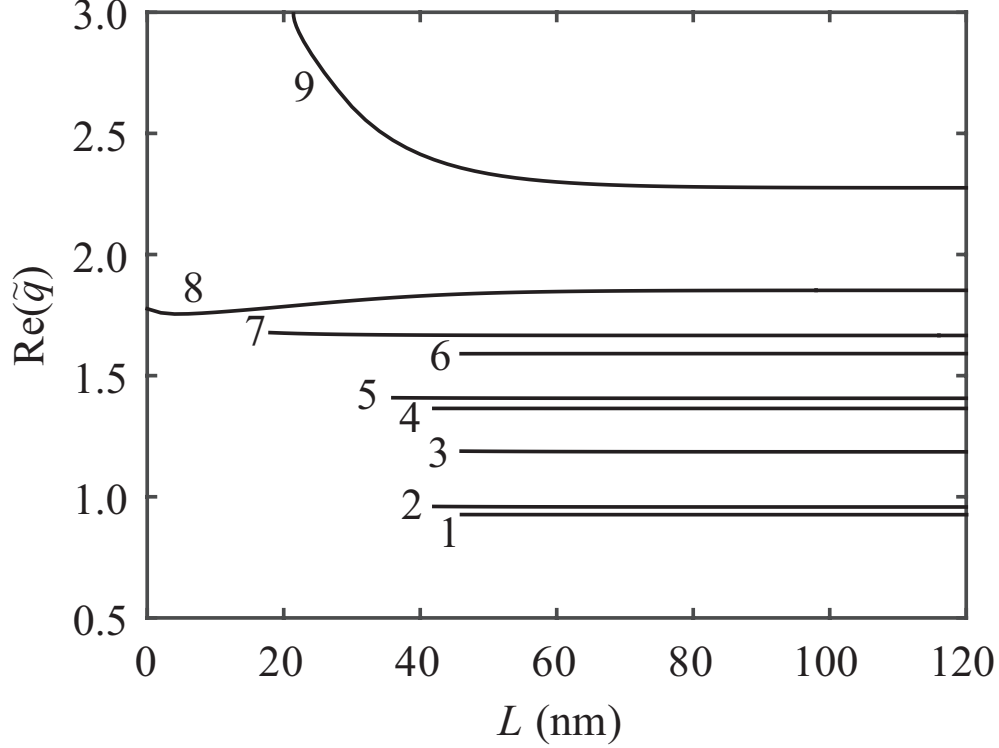


Figure 3: Variation of $\text{Re}(\tilde{q})$ with thickness L of the metal layer for the CGWs guided by PMLID/metal/SCM structure when $\psi = 30$ deg.

For metal thickness L significantly greater than the skin depth $\delta = 26.5$ nm of silver, \tilde{q} and Δ_{prop} assume steady values. Their values for the thickest metal layer considered ($L = 120$ nm) are reported in Table 8. In that table, solutions 1, 4, 6, and 9 are practically the same as for the p -polarized SPP waves guided by the PMLID/metal interface alone (see Table 5); solutions 2, 5, and 7 are almost the same as for the s -polarized SPP waves guided by the PMLID/metal interface alone (see Table 5); and solutions 3 and 8 are almost the same as for the SPP waves guided by planar metal/SCM interface alone (see Table 3). In other words, the PMLID/metal and metal/SCM interfaces in the PMLID/metal/SCM structure are virtually decoupled from each other for $L \gg \delta$.

This decoupling is evident in the spatial distributions of $\mathbf{P}(0, 0, z)$ plotted in Figs. 5, and 6 for solutions 8, and 9 for $L = 120$ nm and $\psi = 30$ deg. The CGWs are bound to either the PMLID/metal interface or the metal/SCM interface, but not to both.

Coupling of the PMLID/metal and metal/SCM interfaces enhances as L is diminished. Each solution branch in Figs. 3 and 4 exists only for $L > L_{th}$, the threshold value L_{th} for each branch (except branch 9) being reported in the last column of Table 8. We were unable to determine L_{th} for solution branch 9, because $\text{Re}(\tilde{q})$ exceeded 3 as L decreased below 21 nm and thus fell out of the range $0 < \text{Re}(\tilde{q}) \leq 3$.

Solution branches 1 to 6 have $L_{th} > \delta = 26.5$ nm, implying relatively weak coupling between the PMLID/metal and metal/SCM interfaces for $L > L_{th}$. Still, Figs. 3 and 4 indicate that \tilde{q} is substantially impacted by the coupling for $L \in [L_{th}, 2\delta]$.

Solution branch 9 exists for $L \approx \delta$, indicating stronger coupling between the two interfaces. This is

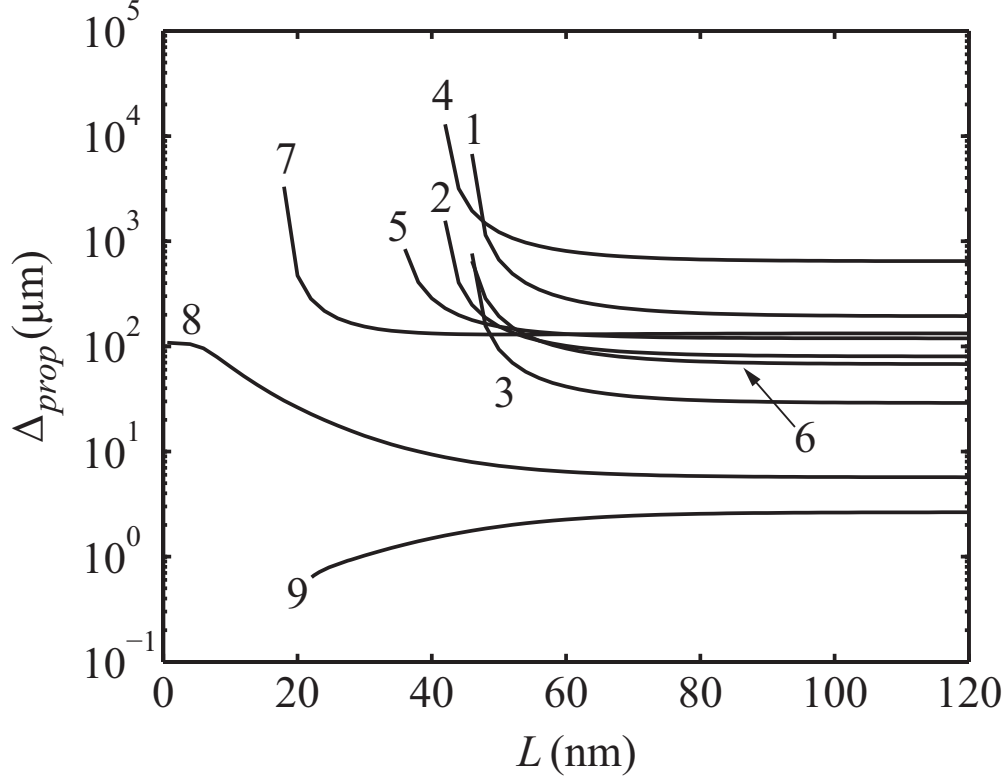


Figure 4: Variation of Δ_{prop} with thickness L of the metal layer for the CGWs guided by PMLID/metal/SCM structure when $\psi = 30$ deg.

Table 8: \tilde{q} , v_{ph} , and Δ_{prop} for CGWs guided by the PMLID/metal/SCM structure when $L = 120$ nm and $\psi = 30$ deg. Solutions with v_{ph} exceeding c_0 are highlighted in bold font. Threshold value L_{th} of the metal thickness below which a solution branch ceases to exist is also reported (correct to the nearest nm), except for solution branch 9.

Soln.	$\text{Re}\{\tilde{q}\}$	$\text{Im}\{\tilde{q}\}$	v_{ph}/c_0	Δ_{prop} (μm)	L_{th} (nm)
1	0.93964	5.19×10^{-4}	1.06424	194.11	46
2	0.95784	1.25×10^{-3}	1.04402	80.60	42
3	1.18554	3.48×10^{-3}	0.84350	28.95	46
4	1.36469	1.56×10^{-4}	0.73277	645.80	42
5	1.40658	8.44×10^{-4}	0.71094	119.37	36
6	1.59093	1.48×10^{-3}	0.62856	68.07	46
7	1.66592	7.57×10^{-4}	0.60027	133.08	18
8	1.85214	1.77×10^{-2}	0.53992	5.69	0
9	2.27538	3.81×10^{-2}	0.43949	2.64	< 21

confirmed by the plots of $\mathbf{P}(0, 0, z)$ versus z for $L = 26$ nm in Fig. 7. Clearly, both the PMLID material and the SCM carry the energy of the CGW, the former more than the latter. Thus, the characteristics of SPP waves of two different types have been mixed in the CGW. SPP waves of one type are guided by the PMLID/metal interface and have specific polarization states, whereas no polarization state can be assigned for SPP waves of the other type as they are guided by the metal/SCM interface [16, 44]. Similar conclusions

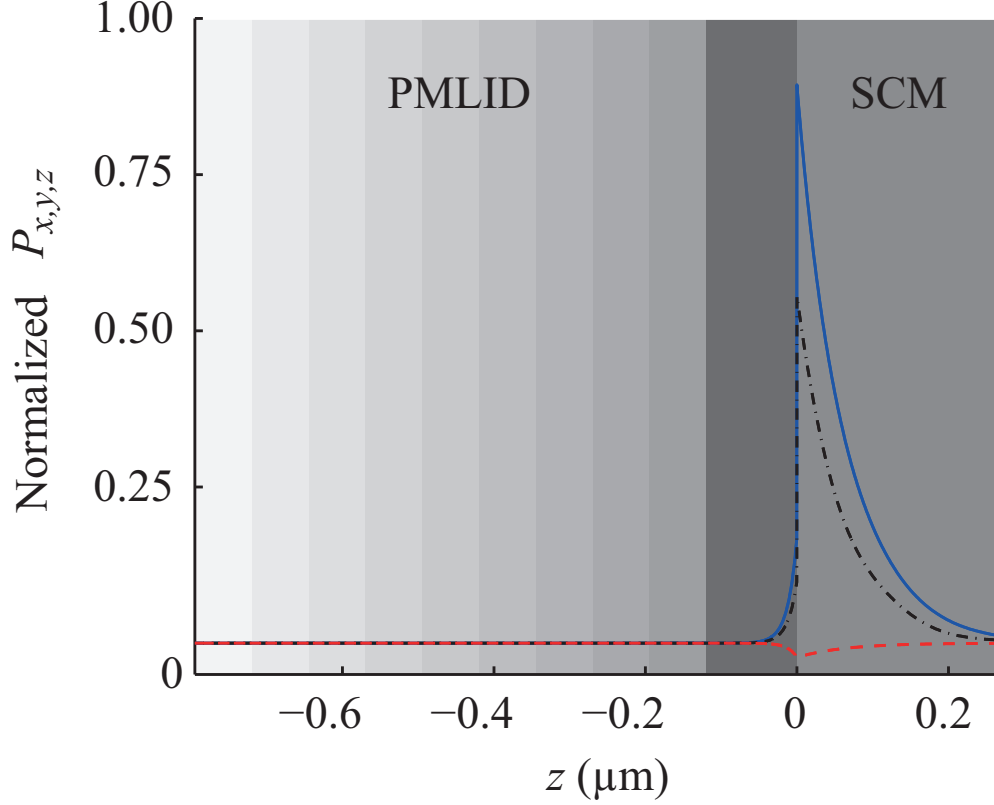


Figure 5: Spatial variations of $P_x(0,0,z)$ (blue solid lines), $P_y(0,0,z)$ (black dashed-dotted lines) and $P_z(0,0,z)$ (red dashed lines) with respect to z for solution 8 of Table 8. The CGW is guided by the PMLID/metal/SCM structure, when $L = 120$ nm and $\psi = 30$ deg.

can be drawn for solution branch 7 as well, for which $L_{th} \approx 0.68\delta$.

Finally, solution branch 8 has $L_{th} = 0$. Hence, solutions must exist even if $L \ll \delta$, which is indicative of very strong coupling between the PMLID/metal and metal/SCM interfaces. The strong coupling is very clear in the spatial profile of $P(0,0,z)$ presented in Fig. 8 for $L = 10$ nm, with the energy of the CGW carried almost equally by the PMLID material and the SCM.

Furthermore, when $L = 0$, the PMLID/metal/SCM structure collapses into the PMLID/SCM structure, \tilde{q} on the solution branch 8 in Figs. 3 and 4 acquires the purely real value 1.77612, the spatial variations of the Cartesian components of the time-averaged Poynting vector $\mathbf{P}(0,0,z)$ of the CGW are the same as presented in Figure 2. and the CGW converts into the Dyakonov–Tamm wave discussed in Sec. 3.7.

4.2 Planar PMLID/dissipative-HID/SCM structure

When material B is the nonplasmonic analog of silver (i.e., $\varepsilon_B = \varepsilon_{dHID} = \varepsilon_{Ag}^*$), as many as five different CGWs can be guided by the PMLID/dissipative-HID/SCM structure for $L \in [0, 120]$ nm and $\psi = 30$ deg. These CGWs for $L > 0$ are compounded from Uller–Zenneck waves of Secs. 3.3 and 3.6; alternatively, they are compounded from the Dyakonov–Tamm waves of Sec. 3.3.3 and the Tamm waves of Sec. 3.6.

Figures 9 and 10 show $\text{Re}(\tilde{q})$ and Δ_{prop} as functions of $L \in (0, 120]$ nm, respectively. The solutions q are organized into five different branches. On every branch, both v_{ph} and Δ_{prop} decrease as L increases. No solutions with phase speed exceeding c_0 were found, most likely because (i) although the PMLID/dissipative-HID interface alone does support high-phase-speed Uller–Zenneck (or Tamm) waves (see

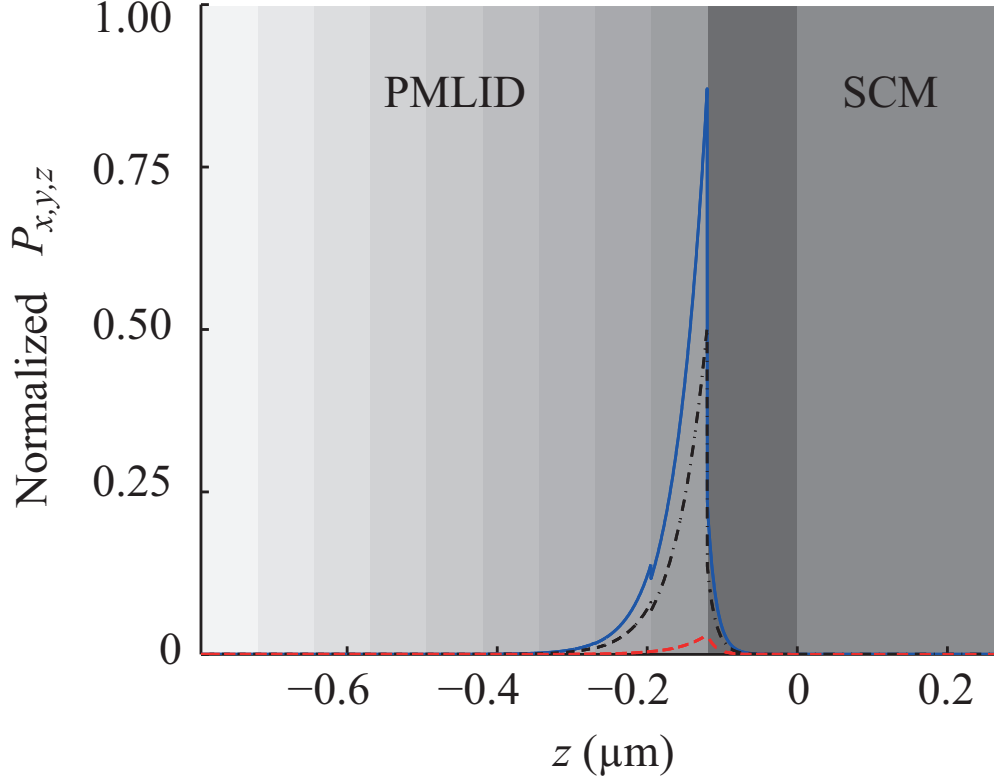


Figure 6: Same as Fig. 5, but for solution 9 of Table 8.

Table 6), the SCM/dissipative-HID interface alone does not support high-phase-speed Uller-Zenneck (or Dyakonov-Tamm) waves (see Table 4, and (ii) L_{max} is much smaller than the skin depth $\delta = 642$ nm in B.

Values of \tilde{q} and Δ_{prop} when $L = 3000$ nm are reported in Table 9. In this table, solutions b and h have values very close to those for two p -polarized Uller-Zenneck waves guided by the PMLID/dissipative-HID interface alone (see Table 6); solutions a , d , and g have values very close to those for the s -polarized Uller-Zenneck waves guided by the PMLID/dissipative-HID interface alone (see Table 6); and solution c has a value very close to that for an Uller-Zenneck wave guided by planar SCM/dissipative-HID interface alone (see Table 4). Solutions e and f in Table 9 are somewhat, but not very, close to a solution in Table 4 and a solution in Table 6, indicating that the two interfaces are coupled even for $L \simeq 4.67\delta$. Their decoupling would require even larger values of the ratio L/δ .

Whereas the number of solution branches is five in Figs. 9 and 10 for $L \leq 120$ nm, the number of solutions is eight in Table 9 for $L = 3000$ nm. Eight must be the largest number of solutions possible, based on the data in Tables 4 and 6. Since each solution branch will exist only for $L > L_{th}$, three solution branches must have $L_{th} \in (120, 3000)$ nm.

Figure 11 present the spatial profiles of $\mathbf{P}(0, 0, z)$ for solution 2 in Figure 9 when $L = 120$ nm. A fraction of the energy of the CGW resides in both the PMLID material and the SCM, with the former carrying more energy than the latter. Clearly then, the characteristics of Uller-Zenneck waves of two different types have been mixed in the CGW. Uller-Zenneck waves of one type (alternatively, Tamm waves) are guided by the PMLID/dissipative-HID interface and have specific polarization states, whereas no polarization state can be assigned for Uller-Zenneck waves of the other type (alternatively, Dyakonov-Tamm waves) as they are guided by the dissipative-HID/SCM interface [28, 16]. Similar conclusions hold for the other four solution branches in Figure 9.

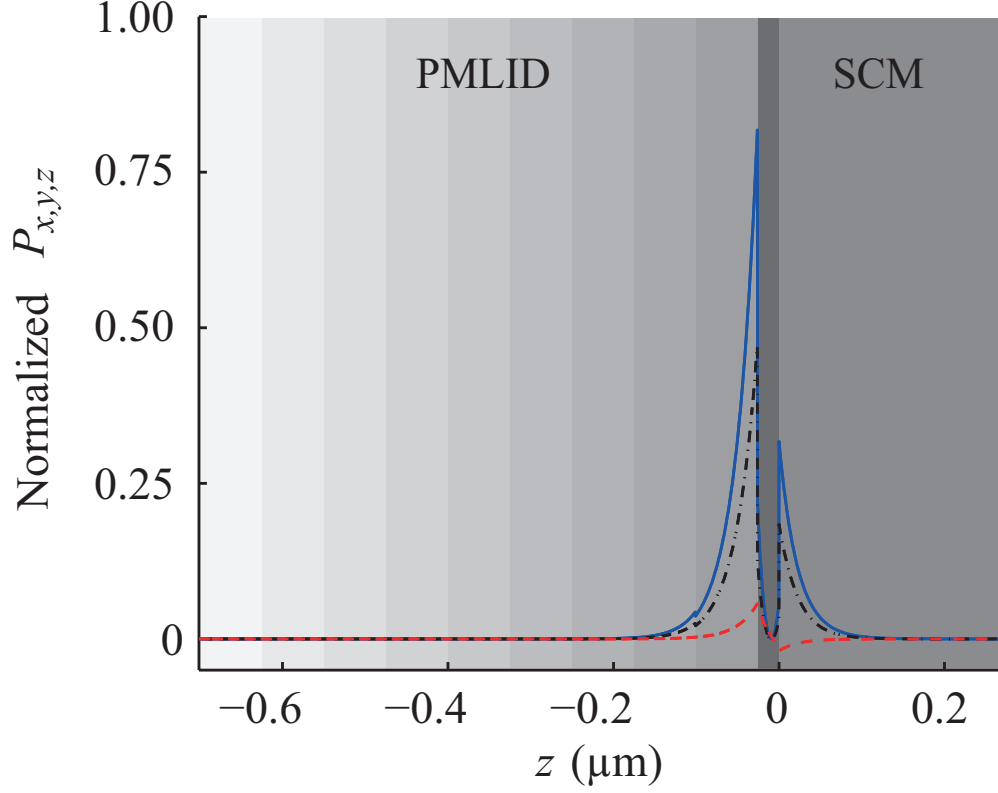


Figure 7: Spatial variations of $P_x(0,0,z)$ (blue solid lines), $P_y(0,0,z)$ (black dashed-dotted lines) and $P_z(0,0,z)$ (red dashed lines) with respect to z for solution branch 9 for the PMLID/metal/SCM structure, when $L = 26$ nm and $\psi = 30$ deg.

Table 9: \tilde{q} , v_{ph} , and Δ_{prop} for CGWs guided by the PMLID/dissipative-HID/SCM structure when $L = 3000$ nm and $\psi = 30$ deg. Solutions with v_{ph} exceeding c_0 are highlighted in bold font.

Soln.	$\text{Re}\{\tilde{q}\}$	$\text{Im}\{\tilde{q}\}$	v_{ph}/c_0	Δ_{prop} (μm)
<i>a</i>	0.91803	6.06×10^{-2}	1.08929	1.66
<i>b</i>	0.92057	3.97×10^{-2}	1.08663	2.54
<i>c</i>	1.06833	5.90×10^{-2}	0.93604	1.71
<i>d</i>	1.38090	3.14×10^{-2}	0.72417	3.21
<i>e</i>	1.51980	5.85×10^{-2}	0.65798	1.72
<i>f</i>	1.52934	5.27×10^{-2}	0.65388	1.91
<i>g</i>	1.64373	2.68×10^{-2}	0.60837	3.76
<i>h</i>	1.71959	1.44×10^{-1}	0.58153	0.70

Only one solution branch in Figs. 9 and 10 has $L_{th} = 0$. Solution 5 is identical to that for the sole Dyakonov–Tamm wave guided by the PMLID/SCM interface by itself in Sec. 3.7.

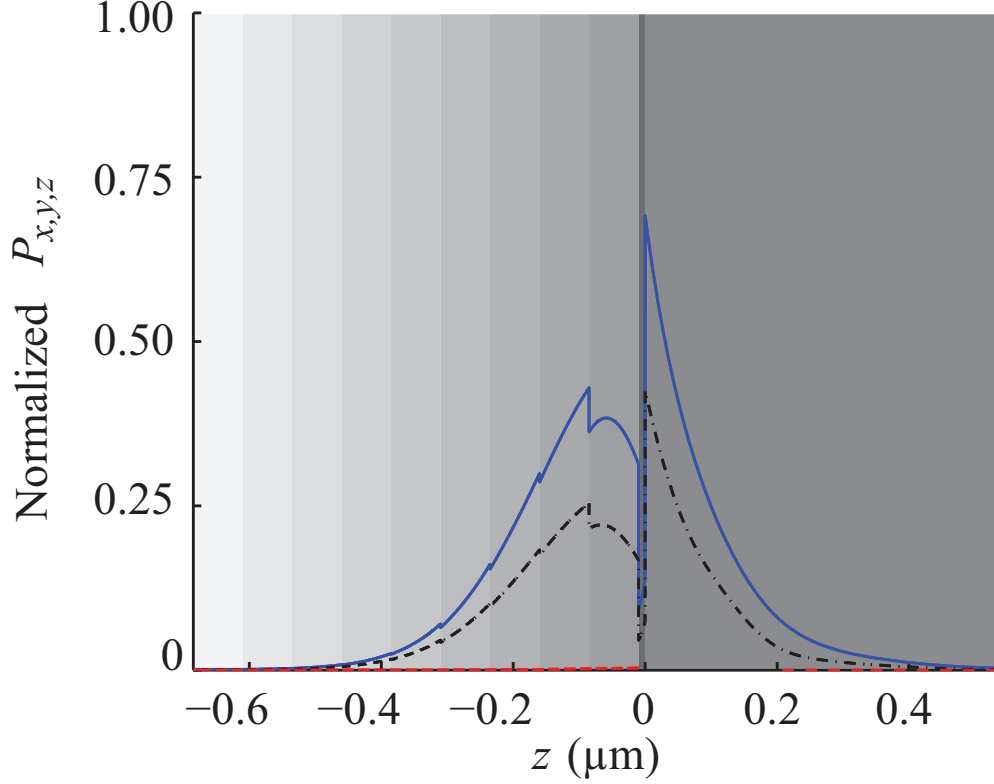


Figure 8: Spatial variations of $P_x(0,0,z)$ (blue solid lines), $P_y(0,0,z)$ (black dashed-dotted lines) and $P_z(0,0,z)$ (red dashed lines) with respect to z for solution branch 8 for the PMLID/metal/SCM structure, when $L = 10$ nm and $\psi = 30$ deg.

4.3 Planar PMLID/nondissipative-HID/SCM structure

When material B is nondissipative (i.e., $\varepsilon_B = \varepsilon_{glass} = 2.56$), only one solution was found in the range $L \in [0, 120]$ nm. Figure 12 depicts \tilde{q} as a function of L . Since all the materials involved are nondissipative \tilde{q} is obviously real-valued so that, theoretically, $\Delta_{prop} \rightarrow \infty$ and the CGW wave can propagate indefinitely. As discussed in Sec. 3.6, there will always be some dissipation so that Δ_{prop} can be large but not infinite.

For a glass layer much thicker than $L_{max} = 120$ nm (i.e., $L = 1000$ nm), two solutions were found. Their values, reported in Table 10, are the same as for the Tamm waves guided by the PMLID/glass interface alone (Table 7) in Sec. 3.6. Solution 2 in Table 10 is the asymptotic value of the curve in Figure 12 as the thickness L of the glass layer increases, whereas solution 1 has obviously a threshold value $L_{th} > 120$ nm.

Table 10: \tilde{q} and v_{ph} for CGWs guided by the PMLID/glass/SCM structure, when $L = 1000$ nm and $\psi = 30$ deg.

Solution	\tilde{q}	v_{ph}/c_0
1	1.72282	0.58044
2	1.74660	0.57254

It is worth pointing out that the solutions found for the PMLID/nondissipative-HID/SCM structure for large L are the same as for the PMLID/nondissipative-HID interface alone. Because the HID is nondissipative

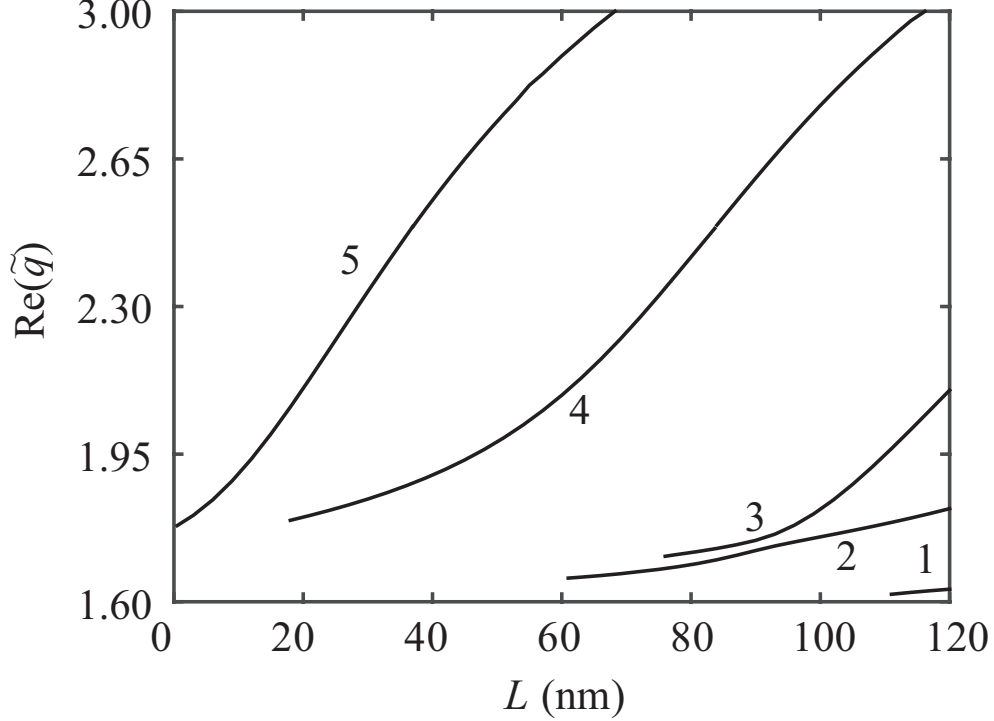


Figure 9: Variation of $\text{Re}(\tilde{q})$ with thickness L of the dissipative-HID layer for the CGWs guided by PMLID/dissipative-HID/SCM structure when $\psi = 30$ deg.

(i.e., the skin depth δ is infinite), this observation means that the coupling between the two interfaces of the sandwiched layer is not only affected by the ratio L/δ but also by the rates at which the fields of the ESWs guided individually by the two interfaces decay away from the respective guiding interfaces.

Even when the skin depth is infinite, a strong coupling between the PMLID/nondissipative-HID and the nondissipative-HID/SCM interfaces is expected for $L \in (0, 120]$ nm. This is confirmed by the plot of $\mathbf{P}(0, 0, z)$ vs. z for $L = 120$ nm in Figure 13. Clearly, both the PMLID and the SCM carry the energy of the CGW, the former more than the latter, and the characteristics of Tamm and Dyakonov–Tamm waves have been mixed in the CGW [16, 28, 19].

5 Concluding remarks

We solved the boundary-value problem for electromagnetic waves guided by a layer of a homogeneous and isotropic (metal or dielectric) material sandwiched between a structurally chiral material and a periodically multi-layered isotropic dielectric material. Though this problem is practically unimplementable *sensu strictissimo* because it involves two half spaces, it provides information on the propagation distance, otherwise unachievable. But it can be implemented in an approximate sense, with a PMLID/sandwiched-material/SCM structure of sufficiently large thickness and finite width interposed between two waveguide sections.

We found that compound guided waves can propagate bound to both interfaces of the sandwiched material with energy distributed in both the SCM and the PMLID materials, if the sandwiched layer is sufficiently thin. Hence, CGWs that mix together the characteristics of SPP waves, Tamm waves, Dyakonov–Tamm waves, and Uller–Zenneck waves are theoretically possible, exemplifying the inherent commonality between these electromagnetic surface waves. A multiplicity of CGWs can exist, depending on the thickness of the sandwiched layer. All of them differ in phase speed, attenuation rate, and field profile, even though all are

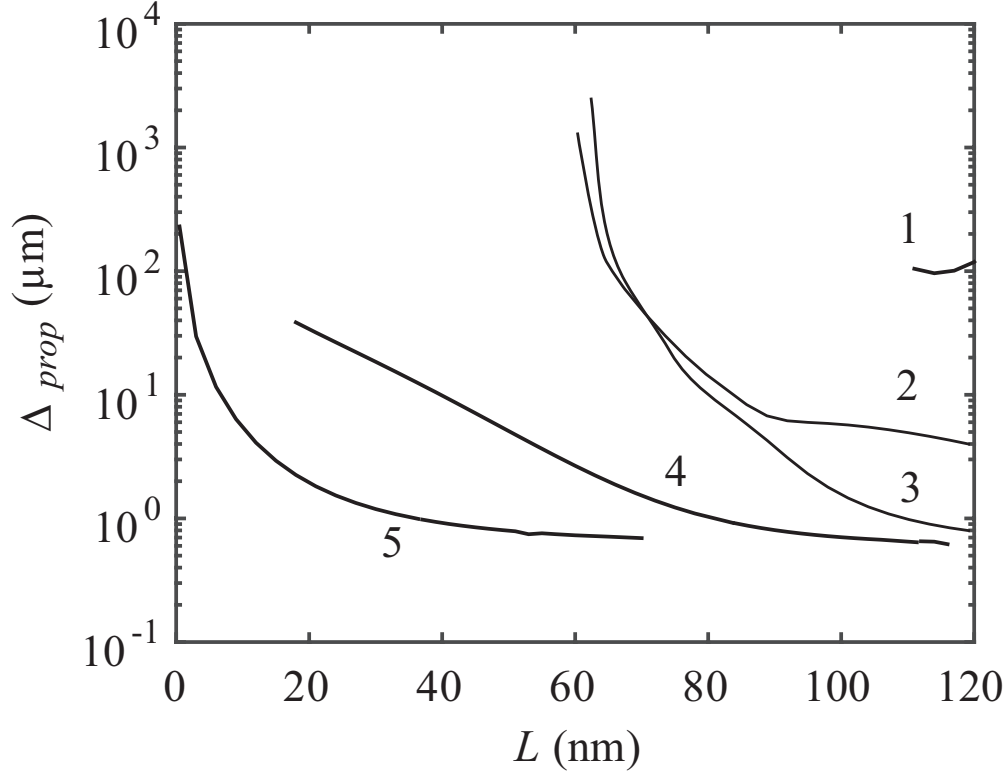


Figure 10: Variation of Δ_{prop} with thickness L of the metal layer for the CGWs guided by PMLID/dissipative-HID/SCM structure when $\psi = 30$ deg.

excitable at the same frequency. For any thickness of the sandwiched layer, at least one CGW exists.

The coupling between the two faces of the sandwiched layer, giving rise to CGWs, is affected by two distinct mechanisms: (i) the ratio of the thickness of the sandwiched layer to the skin depth in that material and (ii) the rates at which the fields of the ESWs guided individually by the two interfaces decay away from their respective guiding interfaces.

Finally, CGWs have been found for an all-dielectric-configuration where the materials used can even be extremely weakly dissipative. Such a configuration could be very useful for sensing applications in special cases where the presence of a metal is unwanted, e.g. in an electrically hazardous environment.

References

- [1] K. Uller, *Beiträge zur Theorie der Elektromagnetischen Strahlung*, Ph.D. thesis (Universität Rostock, 1903), Chap. XIV.
- [2] J. R. Wait, "The ancient and modern history of EM ground-wave propagation," *IEEE Antennas Propagat. Mag.* **40**(5), 7–24 (1998).
- [3] N. Tesla, "Art of transmitting electrical energy through natural mediums," US Patent 787412 (filed on May 16, 1900; published on April 18, 1905).
- [4] J. Zenneck, "Über die Fortpflanzung ebener elektromagnetischer Wellen längs einer ebenen Leiterfläche und ihre Beziehung zur drahtlosen Telegraphie," *Ann. Phys. Lpz.* **23**, 846–866 (1907).

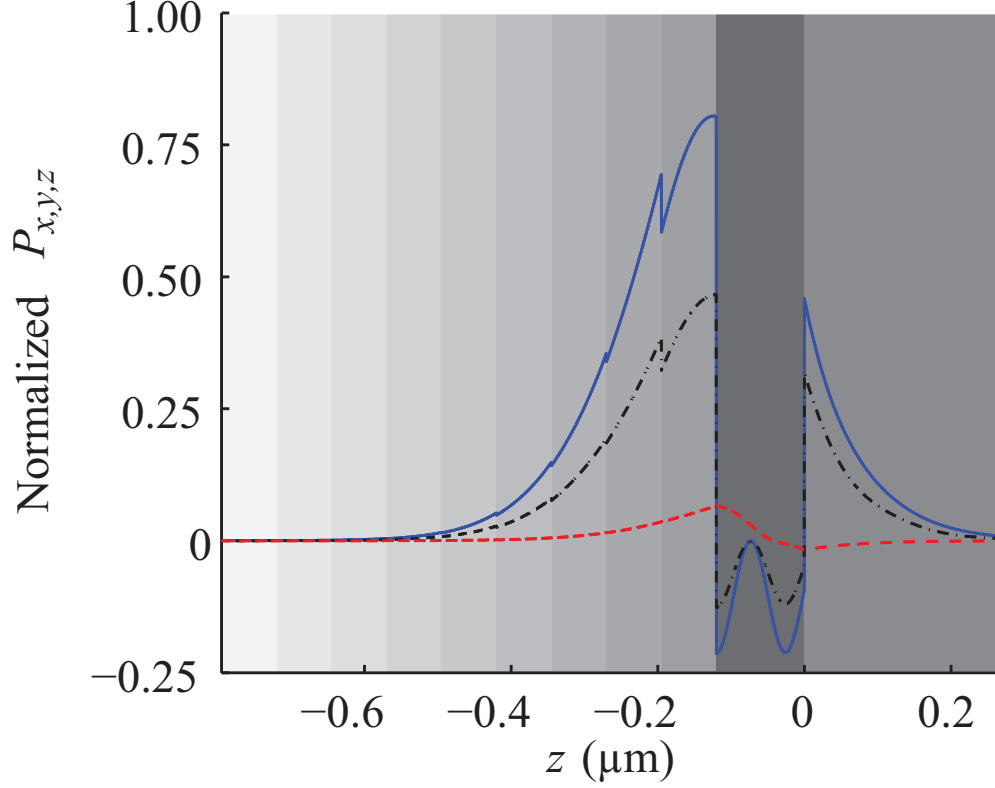


Figure 11: Spatial variations of $P_x(0,0,z)$ (blue solid lines), $P_y(0,0,z)$ (black dashed-dotted lines) and $P_z(0,0,z)$ (red dashed lines) with respect to z for solution 2 guided by the PMLID/dissipative-HID/SCM structure, when $L = 120$ nm and $\psi = 30$ deg.

- [5] A. Sommerfeld, “Über die Ausbreitung der Wellen in der drahtlosen Telegraphie,” Ann. Phys. Lpz. **28**, 665–736 (1909).
- [6] A. Sommerfeld, “Über die Ausbreitung der Wellen in der drahtlosen Telegraphie,” Ann. Phys. Lpz. **62**, 95–96 (1920).
- [7] A. Sommerfeld, “Über die Ausbreitung der Wellen in der drahtlosen Telegraphie,” Ann. Phys. Lpz. **81**, 1135–1153 (1926).
- [8] M. Faryad and A. Lakhtakia, “Observation of the Uller–Zenneck wave”, Opt. Lett. **39**, 5204–5207 (2014).
- [9] R. H. Ritchie, “Plasma losses by fast electrons in thin films,” Phys. Rev. **106**, 874–881 (1957).
- [10] T. Turbadar, “Complete absorption of light by thin metal films,” Proc. Phys. Soc. Lond. **73**, 40–44 (1959).
- [11] A. Otto, “Excitation of nonradiative surface plasma waves in silver by the method of frustrated total reflection,” Z. Phys. **216**, 398–410 (1968).
- [12] E. Kretschmann and H. Raether, “Radiative decay of nonradiative surface plasmons excited by light,” Z. Naturforsch. A **23**, 2135–2136 (1968).

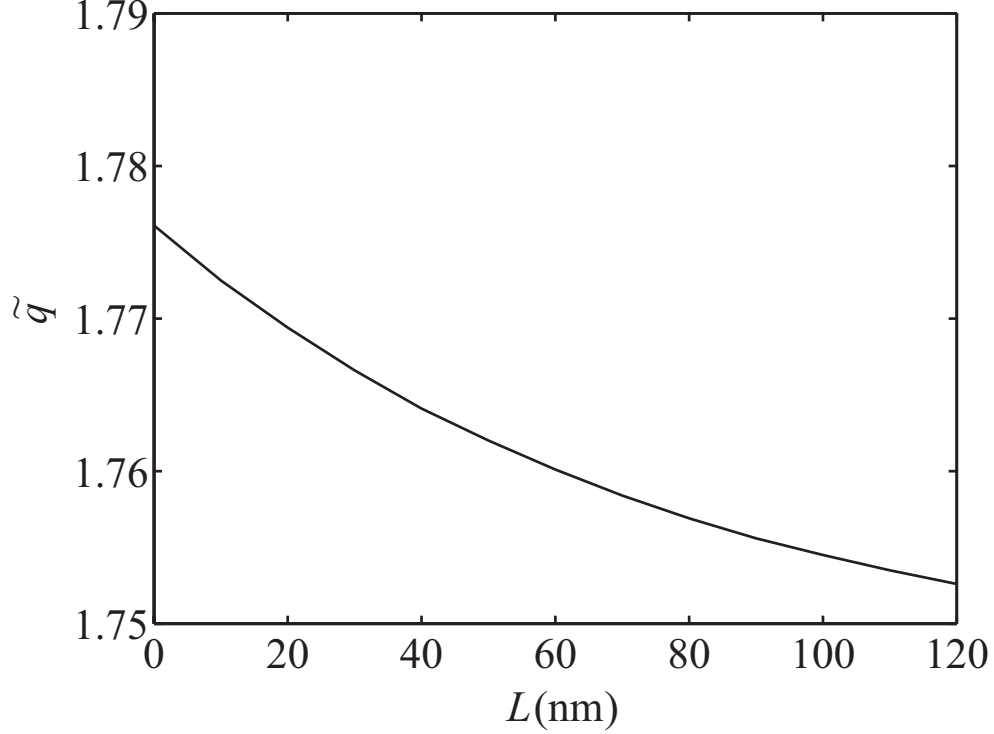


Figure 12: Variation of \tilde{q} with the thickness L of the nondissipative HID layer for the CGW guided by the PMLID/nondissipative-HID/SCM structure when $\psi = 30$ deg.

- [13] J. M. Pitarke, V. M. Silkin, E. V. Chulkov, and P. M. Echenique, “Theory of surface plasmon and surface-plasmon polaritons,” *Rep. Prog. Phys.* **70**, 1–87 (2007).
- [14] I. Abdulhalim, M. Zourob, and A. Lakhtakia, “Surface plasmon resonance for biosensing: A mini-review,” *Electromagnetics* **28**, 214–242 (2008).
- [15] J. Zhang, L. Zhang, and W. Xu, “Surface plasmon polaritons: Physics and applications,” *J. Phys. D: Appl. Phys.* **45**, 113001 (2012).
- [16] J. A. Polo Jr., T. G. Mackay, and A. Lakhtakia, *Electromagnetic Surface Waves: A Modern Perspective*, (Elsevier, Waltham, MA, USA, 2013).
- [17] L. Liu, M. Faryad, A. S. Hall, G. D. Barber, S. Erten, T. E. Mallouk, A. Lakhtakia, and T. S. Mayer, “Experimental excitation of multiple surface-plasmon-polariton waves and waveguide modes in a one-dimensional photonic crystal atop a two-dimensional metal grating,” *J. Nanophoton.* **9**, 093593 (2015).
- [18] G. J. Sprokel, “The reflectivity of a liquid crystal cell in a surface plasmon experiment,” *Mol. Cryst. Liq. Cryst.* **68**, 39–45 (1981).
- [19] P. Yeh, A. Yariv, and C.-S. Hong, “Electromagnetic propagation in periodic stratified media. I. General theory,” *J. Opt. Soc. Am.* **67**, 423–438 (1977).
- [20] P. Yeh, A. Yariv, and A. Y. Cho, “Optical surface waves in periodic layered media,” *Appl. Phys. Lett.* **32**, 104–105 (1978).
- [21] M. Shinn and W. M. Robertson, “Surface plasmon-like sensor based on surface electromagnetic waves in a photonic band-gap material,” *Sens. Actuat. B: Chem.* **105**, 360–364 (2005).

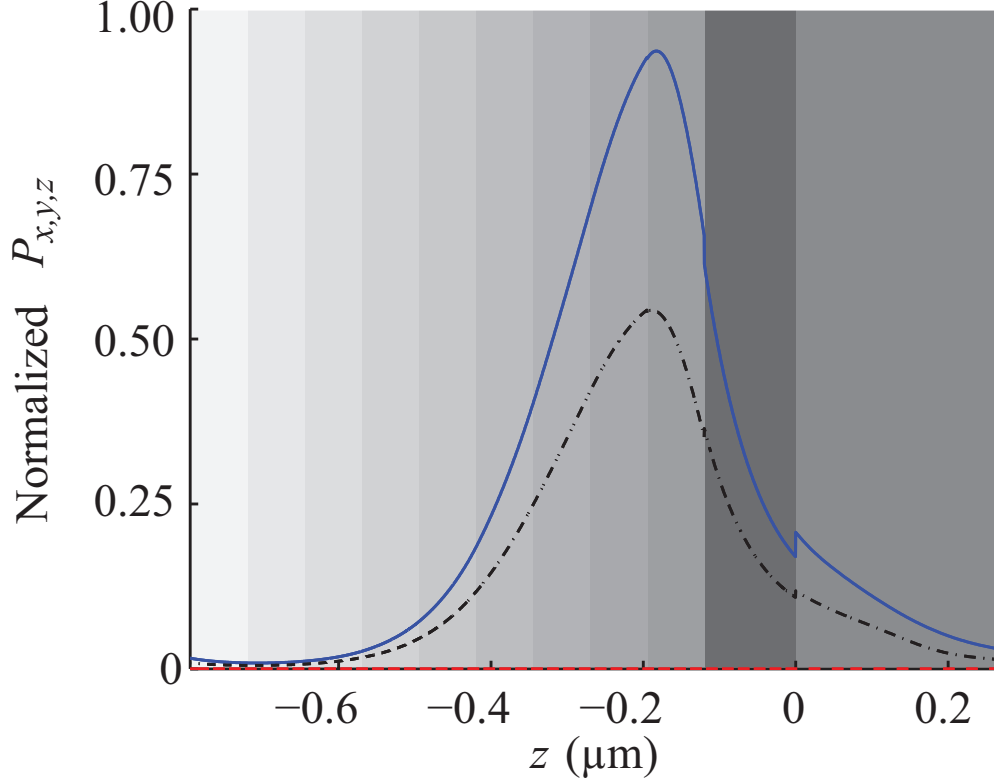


Figure 13: Spatial variations of $P_x(0, 0, z)$ (blue solid lines), $P_y(0, 0, z)$ (black dashed-dotted lines) and $P_z(0, 0, z)$ (red dashed lines) with respect to z for the PMLID/glass/SCM structure, when $L = 120$ nm and $\psi = 30$ deg.

- [22] V. N. Konopsky and E. V. Alieva, “Photonic crystal surface waves for optical biosensors,” *Anal. Chem.* **79**, 4729–4735 (2007).
- [23] F. N. Marchevskii, V. L. Strizhevskii, and S. V. Strizhevskii, “Singular electromagnetic waves in bounded anisotropic media,” *Sov. Phys. Solid State* **26**, 911–912 (1984).
- [24] M. I. D’yakonov, “New type of electromagnetic wave propagating at an interface,” *Sov. Phys. JETP* **67**, 714–716 (1988).
- [25] O. Takayama, L. Crasovan, D. Artigas, and L. Torner, “Observation of Dyakonov surface waves,” *Phys. Rev. Lett.* **102**, 043903 (2009).
- [26] O. Takayama, L.-C. Crasovan, S. K. Johansen, D. Mihalache, D. Artigas, and L. Torner, “Dyakonov surface waves: A review,” *Electromagnetics* **28**, 126–145 (2008).
- [27] O. Takayama, D. Artigas, and L. Torner, “Lossless directional guiding of light in dielectric nanosheets using Dyakonov surface waves,” *Nature Nanotechnol.* **9**, 419–424 (2014).
- [28] A. Lakhtakia and J. A. Polo Jr., “Dyakonov–Tamm wave at the planar interface of a chiral sculptured thin film and an isotropic dielectric material,” *J. Eur. Opt. Soc. Rapid Publ.* **2**, 07021 (2007).
- [29] A. Lakhtakia and M. Faryad, “Theory of optical sensing with Dyakonov–Tamm waves,” *J. Nanophoton.* **8**, 083072 (2014).

- [30] E. N. Economou, “Surface plasmons in thin films,” *Phys. Rev.* **182**, 539–554 (1969).
- [31] L. Wendler and R. Haupt, “An improved virtual mode theory of ATR experiments on surface polaritons: Application to long-range surface plasmon-polaritons in asymmetric layer structures,” *phys. stat. sol. (b)* **143**, 131–148 (1987).
- [32] F. Yang, J. R. Sambles, and G. W. Bradberry, “Long-range surface modes supported by thin films,” *Phys. Rev. B* **44**, 5855–5872 (1991).
- [33] F. Chiadini, V. Fiumara, A. Scaglione, and A. Lakhtakia, “Composite surface-plasmon-polariton waves guided by a thin metal layer sandwiched between a homogeneous isotropic dielectric material and a periodically multilayered isotropic dielectric material,” *J. Nanophoton.* **9**, 093060 (2015).
- [34] F. Chiadini, V. Fiumara, A. Scaglione, and A. Lakhtakia, “Compound surface-plasmon-polariton waves guided by a thin metal layer sandwiched between a homogeneous isotropic dielectric material and a structurally chiral material,” *Opt. Commun.* **363**, 201–206 (2016).
- [35] M. Faryad and A. Lakhtakia, “Multiple surface-plasmon-polariton waves localized to a metallic defect layer in a sculptured nematic thin film,” *Phys. Status Sol. RRL* **4**, 265–267 (2010).
- [36] M. Faryad and A. Lakhtakia, “Propagation of surface waves and waveguide modes guided by a dielectric slab inserted in a sculptured nematic thin film,” *Phys. Rev. A* **83**, 013814 (2011).
- [37] O. Takayama, D. Artigas, and L. Torner, “Coupling plasmons and dyakonons,” *Opt. Lett.* **37**, 1983–1985 (2012).
- [38] P. W. Baumeister, *Optical Coating Technology* (SPIE Press, Bellingham, WA, USA, 2004).
- [39] I. J. Hodgkinson and Q. h. Wu, *Birefringent Thin Films and Polarizing Elements* (World Scientific, Singapore, 1997).
- [40] A. Lakhtakia and R. Messier, *Sculptured Thin Films: Nanoengineered Morphology and Optics* (SPIE, Bellingham, WA, USA, 2005).
- [41] P. G. de Gennes and J. A. Prost, *The Physics of Liquid Crystals, 2nd ed.* (Clarendon Press, Oxford, United Kingdom, 1993).
- [42] M. Faryad, A. S. Hall, G. D. Barber, T. E. Mallouk, and A. Lakhtakia, “Excitation of multiple surface-plasmon-polariton waves guided by the periodically corrugated interface of a metal and a periodic multilayered isotropic dielectric material,” *J. Opt. Soc. Am. B* **29**, 704–713 (2012).
- [43] I. Hodgkinson, Q. h. Wu, and J. Hazel, “Empirical equations for the principal refractive indices and column angle of obliquely deposited films of tantalum oxide, titanium oxide, and zirconium oxide,” *Appl. Opt.* **37**, 2653–2659 (1998).
- [44] J. A. Polo Jr., T. G. Mackay, and A. Lakhtakia, “Mapping multiple surface-plasmon-polariton-wave modes at the interface of a metal and a chiral sculptured thin film,” *J. Opt. Soc. Am. B* **28**, 2656–2666 (2011).
- [45] M. R. M. Atalla, M. Faryad, and A. Lakhtakia, “On surface-plasmon-polariton waves guided by the interface of a metal and a rugate filter with a sinusoidal refractive-index profile. Part II: High-phase-speed solutions,” *J. Opt. Soc. Am. B* **29**, 3078–3086 (2012).